OUKA
The University of Osaka
Institutional Knowledge Archive

Title	Hydrodynamics of collisional structures in laser-produced plasmas
Author(s)	Vick, D.; Kado, M.; Yamamoto, H. et al.
Citation	Physical Review E. 1993, 48(3), p. 2308-2311
Version Type	VoR
URL	https://hdl.handle.net/11094/2913
rights	Vick, D., Kado, M., Yamamoto, H., Nishiguchi, A., Tanaka, K.A., Mima, K., Offenberger, A.A., Capjack, C.E., Nakai, S., Physical Review E, 48, 3, 2308-2311, 1993-09. "Copyright 1993 by the American Physical Society."
Note	

The University of Osaka Institutional Knowledge Archive : OUKA

https://ir.library.osaka-u.ac.jp/

The University of Osaka

Hydrodynamics of collisional structures in laser-produced plasmas

D. Vick
Department of Electrical Engineering, University of Alberta, Edmonton, Alberta, Canada T6G 2G7

M. Kado, H. Yamamoto, and A. Nishiguchi
Institute of Laser Engineering, Osaka University, Yamadaoka 2-6, Suita, Osaka 565, Japan

K. A. Tanaka
Department of Electromagnetic Energy Engineering, Osaka University, Yamada-oka 2-1, Suita, Osaka 565, Japan

K. Mima
Institute of Laser Engineering, Osaka University, Yamada-oka 2-6, Suita, Osaka 565, Japan

A. A. Offenberger and C. E. Capjack
Department of Electrical Engineering, University of Alberta, Edmonton, Alberta, Canada T6G 2G7

S. Nakai
Institute of Laser Engineering, Osaka University, Yamada-oka 2-6, Suita, Osaka 565, Japan
(Received 8 March 1993)

The formation and evolution of collisional structures in the coronas of laser-produced plasmas have been studied by irradiating multilayered targets with nonuniform laser beams. Spatially resolved x-ray emission patterns and spectra were recorded to infer the temperatures, ionization states, and time-integrated hydrodynamic histories of plasmas originating from tracer layers embedded in the targets. The conditions of the experiment have been simulated using a two-dimensional single-fluid hydrodynamic code. The experimental results and code predictions are in good agreement, showing the stagnation of colliding plasmas in the nonirradiated regions.

PACS number(s): 52.25.Nr

The study of hydrodynamic structures in the corona of laser-produced plasmas continues to attract the attention of researchers in the field of inertial confinement fusion, for which driver uniformity remains a key issue. Radiative-cooling instabilities are prime candidates for explaining the relatively cool, high-density jets that have been observed in the blowoff plasma during the later stages of the laser pulse [1]. Even more serious for the uniformity issue are structures that exist at or form during the early phase of target compression. Recent simulation studies [2] and x-ray imaging measurements from the ablation region of targets [3] indicate that initial beam nonuniformities can create density structures that persist throughout the laser pulse. If such structures extend into the corona, filamentation and self-focusing effects may result [4]. The related subject of colliding and interpenetrating plasmas has attracted research directed toward the aim of achieving suitable conditions for x-ray amplification or directed x-ray transport. Previous experiments have incorporated a variety of beam-target configurations including dual beam and parallel planar targets [5,6], split beam and single planar targets [7], and single beam and internally-irradiated microtubes [8]. In conjunction with experimental studies, numerical modeling has been able to reproduce observed features of the plasma, such as the temperature, density, and emissivity [7,9,10].

This article describes an experiment in which collisional structures in the expanding corona of laser-produced plasmas were deliberately created by imposing irradiation nonuniformities onto planar targets. The experiments were performed by using a single beam of the Gekko IV neodymium glass laser at the Institute of Laser Engineering of Osaka University. Gaussian-shaped pulses [full width at half maximum (FWHM) 900 ps] were frequency doubled by a type-II potassium diphosphate crystal to produce 0.53-μm radiation with typical energies 1–10 J. An $f/2$ plano-convex lens focused the laser at near-normal incidence onto planar polystyrene (CH) targets of thickness 15 μm.

The nonuniform irradiation conditions at the target surface were produced by a set of opaque strips positioned in the beam prior to the focusing lens, while the target was positioned 310 μm on the convergent side of best focus. The resulting focal spot consisted of alternating strips of high and low intensity of equal width (56 μm) superimposed within a nominal focal-spot diameter of 300 μm. Most of the laser energy was deposited in two strips positioned symmetrically on either side of the beam axis. In order to study the time history of the corona, the technique of buried tracer layers was adopted [11]. The tracers consisted of 400-μm-diameter aluminum discs vacuum deposited to a thickness of 1000 Å onto the target substrates and overcoated with varying depths (0–1 μm) of parylene (CH). The laser spot was positioned to fall entirely within the tracer area.

 ©1993 The American Physical Society

The time-integrated x-ray emission from the tracer targets was imaged with a pinhole camera of resolution 20 μm, dispersed with a Bragg reflecting-crystal spectrometer, and recorded with Kodak DEF film. The pinhole camera viewed the target laterally along a line of sight parallel to the irradiation strips, while the line of sight of the spectrometer subtended an angle of 36° with respect to target normal. A 35-μm spectrometer entrance slit enabled lateral resolution of the emission spectra across the intensity modulations. Both instruments incorporated Be foil windows which filtered out radiation below an effective cutoff energy of 1 keV. For the conditions of these experiments, the majority of the CH-emission plasma is attenuated by the Be filter and the instruments record primarily aluminum emission above the cutoff energy. By using targets of varying CH overcoat thicknesses one therefore records the time-integrated history of tracer material originating from specific depths in the target.

In Fig. 1 we present x-ray pinhole images from four targets of varying overcoat thickness. The laser propagates from the right, converging with a beam f number of 2. The recorded energy on target for all of these shots fell within the range 9.6 ± 0.6 J, with corresponding peak intensities of 3.3×10^{13} W/cm^2 in the irradiated areas. The CH overcoat thicknesses for the images range from 0.54 to 0.0 μm (the maximum ablation depth for CH targets under these irradiation conditions is ~1.6 μm). In the case of the target with thickest overcoat [Fig. 1(a)], the emission features consist primarily of the hot expansion plumes of the directly irradiated regions. As the overcoat thickness is progressively decreased, forklike emission structures are observed in the nonirradiated or "shadow" regions of the target. These features become the three dominant flame shapes in the case of the uncoated target [Fig. 1(d)].

The spatial features of the spectrometer data exhibit the same characteristics as the pinhole images. For overcoated targets, the emission features originate primarily from the irradiated regions. The lateral widths of these features increase as the overcoat thickness is decreased. For uncoated targets a bright aluminum spectrum is recorded in the low-intensity region. Typical spectra are presented in Fig. 2. Spectrum 2(a) was recorded from the same shot as pinhole image 1(a) and represents the emission features of the laser-irradiated region. Figure 2(b) shows a spectrum for a 4.9-J shot on an uncoated target. This spectrum originates from the nonirradiated region of the target, and exhibits evidence of strong recombination into the continumm and upper levels of hydrogenlike and heliumlike aluminum. Using published information for the film sensitivity, crystal reflectivity, and Be-filter attenuation [12], theoretical spectra generated by the RATION code [13] were fitted to the experimental spectra of Fig. 2, resulting in characteristic temperature and electron-density estimates for the emitting plasma of 580 eV and 4.0×10^{20} cm^{-3} for the case of 2(a), and 560 eV and 2.0×10^{20} cm^{-3} for the case of 2(b). The best fit for the latter spectrum was obtained if a plasma length of 50-μm extent was assumed in order to account for opacity effects. This assumption is in accord with the pinhole images, which indicate that this spectrum originates from a comparatively extended region. The temperature and density estimates obtained from 2(b) must be viewed as tentative only since the equilibrium conditions assumed by the RATION code may not prevail in the shadow region. The emission from the irradiated region of shot 2(b) was not well characterized by a single temperature or density. This may be expected since the tracer layer progressed through a wide range of conditions during the early part of the laser pulse.

We interpret the emission features in the nonirradiated areas as evidence for stagnation in the collision of hot coronal plasmas undergoing lateral expansion from the laser-irradiated regions. For uncoated targets, the aluminum tracer layer ablates first, expanding and colliding to produce the flame-shaped features of Fig. 1(d). In the case of the CH-overcoated targets, the overcoat layer ablates first, forming the dark inner structures of the forks, which widen as the CH overcoating increases; the emission from these structures is filtered out by the instruments. The boundaries between the dark and bright features of the collisional region are quite distinct. This cannot be accounted for by the opacity of the CH, which is essentially fully ionized under these conditions, and suggests that there is little interpenetration of the colliding plasmas.

In order to support the foregoing interpretation of the

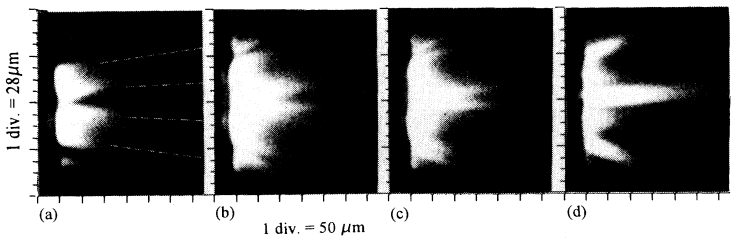

FIG. 1. Time-integrated x-ray pinhole images from four CH-Al-CH layered targets irradiated by a nonuniform laser beam of spatial periodicity 112 μm. The x-ray emission originates primarily from the aluminum layer, which was buried at depths of 0.54, 0.24, 0.12, and 0.0 μm for targets (a)–(d), respectively. The laser converged from the right with $I_{peak}=3.3\times10^{13}$ W/cm^2 $\pm6\%$ and FWHM = 860 ps [the dashed lines in (a) indicate the two main irradiated regions]. Emission from collisional plasmas in the nonirradiated regions become increasingly predominant as the depth of the first CH layer decreases, resulting in the three flame-shaped prominences in the case of (d).

data, several simulations were run on the two-dimensional (2D) single-fluid hydrodynamic code IZANAMI. This code is based on an improved particle-in-a-cell implementation of the Navier-Stokes equations [14], and incorporates a diffusion model for radiation transport and an average ion model for the atomic physics [15]. Generation of magnetic fields and their inhibiting effect on electron thermal transport is also included. For the simulations discussed here a flux limiter of 0.1 was imposed on the thermal transport along both directions.

The simulations were run for laser intensities corresponding to Fig. 1, with fluid particles of CH and Al initially distributed to simulate the various targets used in the experiments. A Cartesian grid with lateral dimension equal to the spatial periodicity of the intensity modulations (112 μm) was used. The laser energy is deposited in the central 56 μm of the lateral domain, and a reflective boundary condition was applied at those boundaries parallel to the laser axis, enforcing a stagnation of the lateral component of the hydroflow there. This single-fluid model for the plasma collision is adequate for distances within 100 μm of the target surface and all but the earliest times of the plasma collision; the ion flow into these boundaries is characterized by lateral velocities and densities which result in stopping distances on the order of a μm.

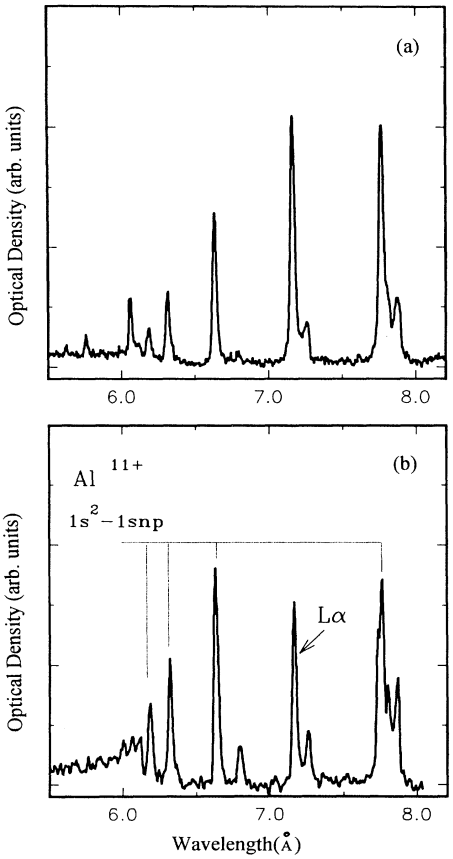

FIG. 2. K-shell x-ray spectra recorded from the expanding aluminum layer of the targets. 2(a) was recorded from the irradiated region of a 0.54-μm overcoated target; spectrum 2(b) was recorded from the nonirradiated region of an uncoated target, and exhibits strong recombination into the upper levels of highly ionized aluminum ions.

Contour plots of the average ionization state at four different simulation times are shown in Fig. 3 for a simulation with laser and target parameters of Fig. 1(d). The plots have been reflected about one of the stagnation boundaries to facilitate comparison with the pinhole image. The ionization contours from $Z=2$ to 10 span the range from weakly ionized CH to highly ionized Al, and the region $Z>8$ may be interpreted as the predicted time history of the emitting tracer. Taking as convention $t=0$ ps at the moment of peak laser intensity, the plots represent $t=-840$, -390, $+60$, and $+810$ ps, respectively. At the beginning of the pulse ($t=-1290$ ps), the ablated material from the laser-heated region quickly undergoes a 2D expansion and reaches the lateral boundary at -800 ps. After collision, the partially stagnated plasma continues to move from the target at a slower rate than the plume in the laser-heated region. The relative longevity of the stagnated plasma would account in part for the brightness of this feature as recorded by the time-integrating diagnostics. In simulations of CH-overcoated targets a well-defined Al-CH-Al sandwich forms at boundaries, and persists as it flows away from the target.

Emissivity spectra generated by IZANAMI were convolved with the filter response of the pinhole diagnostic, and integrated over energy and time to produce spatial emissivity patterns. The spatial structures of these calculated patterns are in qualitative agreement with the pinhole images, with the dominant emission feature shifting from the irradiated region to the shadow region as the CH overcoating is decreased. For the case of the 0.54-μm-overcoated target the 50% emissivity region is enclosed by an unbroken contour of lateral width 43 μm situated in the irradiated region; for the case of the 0.12-μm-overcoated target the same contour is broken into two curves (combined width 23 μm) lying adjacent to the stagnation boundaries. Predicted density and electron-temperature profiles exhibit moderate lateral variation after the collisional plasma has formed. Although the

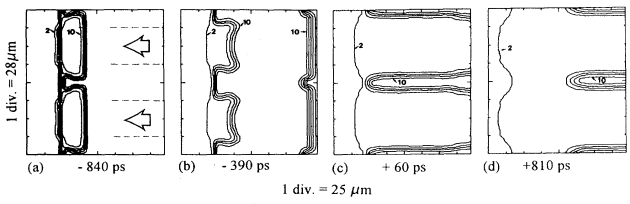

FIG. 3. Average ionization states from $Z=2$ to 10 as predicted by the 2D code IZANAMI for the experimental conditions of Fig. 1(d). A region of highly stripped aluminum ($Z>8$) may be seen to form in the nonirradiated regions early during the pulse, and persist after the laser peak is reached ($t=0$ ps). The plots have been reflected about one of the stagnation boundaries to facilitate comparison with the pinhole image and the irradiated regions of the simulation indicated by the arrows in (a).

fluid collision results in ion temperatures exceeding 1 keV, thermal transport during the laser pulse is electron dominated since the equipartition time between the two species is several times the laser-pulse length. A high degree of lateral thermal smoothing is achieved despite the inhibitory effect of the magnetic-field structures. These reach peak values of $\sim 3\times 10^5$ G in the coronal boundary between the irradiation and shadow regions, and reduce the lateral thermal conductivity by 5–50%. Electron temperatures in the collisional region are about 100 eV lower during the rising part of the pulse. Lateral thermalization continues throughout the pulse and is established by $t = 500$ ps. Electron temperatures in the directly heated region peak at about 600 eV at a distance of 100 μm from the target, in good agreement with the estimates obtained from the x-ray spectrum. Interpretation of lateral density profiles requires some care since both tracer and substrate materials are involved in the simulation. At times for which only one species exists in the corona, the density of the collisional region is moderately higher but never exceeds that of the heated region by more than a factor of 1.5.

In summary, the technique of tracer layers has been used to study the formation and evolution of coronal structures under non-uniform irradiation conditions. X-ray emission from the nonirradiated region clearly shows a stagnation in the lateral collision of expanding plasmas created in the laser-irradiated regions. Good agreement between experimental measurements and 2D simulations has been demonstrated, consistent with the assumption of lateral stagnation in the collisional region.

The authors wish to thank H. Sugio, T. Hagihara, and T. Sakamoto for technical assistance in the operation of Gekko IV, and M. Takagi for help in fabrication of the targets. This work was funded in part by the International Communications Foundation and the Natural Science and Engineering Research Council of Canada.

[1] L. J. Dhareshwar *et al.*, Phys. Fluids B **4**, 1635 (1992), and references therein.
[2] M. Desselberger *et al.*, Phys. Rev. Lett. **68**, 1539 (1992).
[3] M. H. Emery *et al.*, Phys. Fluids B **3**, 2640 (1991).
[4] A. J. Schmitt, Phys. Fluids B **3**, 3079 (1988).
[5] P. Glas *et al.*, Opt. Commun. **86**, 271 (1991); P. Glas and M. Schnürer, Laser Part. Beams **9**, 501 (1991).
[6] R. A. Bosch *et al.*, Phys. Fluids B **4**, 979 (1992).
[7] U. Sh. Begimkulov *et al.*, Kvant. Elektron. (Moscow) **18**, 877 (1991) [Sov. J. Quantum Electron **21**, 794 (1991)].
[8] C. Stöckl and G. D. Tsakiris, Laser Part. Beams **9**, 725 (1991), and references therein.
[9] R. L. Berger *et al.*, Phys. Fluids B **3**, 3 (1991).
[10] S. M. Pollaine, R. L. Berger, and C. J. Keane, Phys. Fluids B **4**, 989 (1992).
[11] M. J. Herbst *et al.*, Rev. Sci. Instrum. **53**, 1418 (1982).
[12] B. L. Henke, J. Y. Uejio, G. F. Stone, C. H. Dittmore, and F. C. Fujiwara, J. Opt. Soc. Am. B **3**, 1540 (1986); B. L. Henke, P. Lee, J. Tanaka, R. L. Shimabukuro, and B. K. Fujiwara, At. Data Nucl. Data Tables **27**, 1 (1982).
[13] R. W. Lee and B. L. Whitten, J. Quant. Spectrosc. Radiat. Transfer **32**, 91 (1984).
[14] A. Nishiguchi and T. Yabe, J. Comput. Phys. **52**, 390 (1983).
[15] M. Itoh, T. Yabe, and S. Kiyokawa, Phys. Rev. A **35**, 233 (1987).

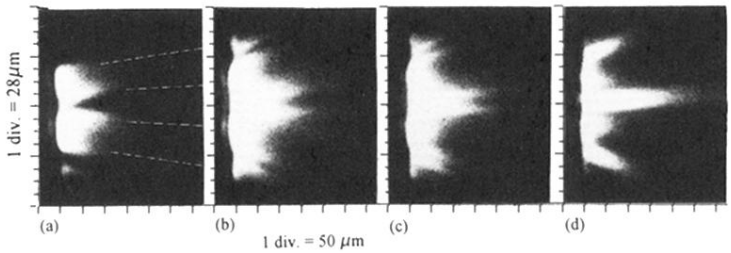

FIG. 1. Time-integrated x-ray pinhole images from four CH-Al-CH layered targets irradiated by a nonuniform laser beam of spatial periodicity 112 μm. The x-ray emission originates primarily from the aluminum layer, which was buried at depths of 0.54, 0.24, 0.12, and 0.0 μm for targets (a)–(d), respectively. The laser converged from the right with $I_{\text{peak}} = 3.3 \times 10^{13}$ W/cm^2 $\pm 6\%$ and FWHM $= 860$ ps [the dashed lines in (a) indicate the two main irradiated regions]. Emission from collisional plasmas in the nonirradiated regions become increasingly predominant as the depth of the first CH layer decreases, resulting in the three flame-shaped prominences in the case of (d).